

Originally published in: Journal of Marine Science  
and Technology, volume 11, pp. 123–130 (2006)

The original publication is available at [springerlink.com](http://springerlink.com)  
and directly at <http://dx.doi.org/10.1007/s00773-005-0208-z>

Copyright: The Japan Society of Naval Architects and Ocean Engineers

# Underwater acoustic imaging: image due to a specular reflector in the geometrical-acoustics limit<sup>1</sup>

DAVID G. BLAIR

Ocean Technology Group J05, Department of  
Civil Engineering, University of Sydney,  
Sydney, NSW 2006, Australia  
(D.Blair@civil.usyd.edu.au)

**Abstract:** In underwater acoustic imaging, used to produce high-quality images in turbid waters, a specular reflector can produce a ‘pseudoimage’ of the receiving array at the reflecting surface. Based on the ‘geometrical approximation’ (similar to geometrical acoustics), formulae are derived for the size and shape of the pseudoimage for both flat and curved reflectors. For curved reflectors, described by two principal radii of curvature, the formulae assume also the ‘large-range approximation.’ The formulae enable radii of curvature to be determined from an image. Also discussed briefly are possible extensions and the role of non-geometrical effects.

**Key words:** Acoustic imaging · Specular reflector · Acoustic array · Geometrical acoustics · Radius of curvature

---

<sup>1</sup>Received: May 9, 2005 / Accepted: September 8, 2005

# 1 Introduction

There are many situations where it would be advantageous to have high-quality images in turbid waters. In sediment-laden waters, visual or video-camera observation is rendered useless. To address this problem, in 1991 an innovation program was initiated by the Australian Defence Science and Technology Organisation (DSTO); this program has been outlined by Jones.<sup>1</sup> Partners in this underwater acoustic imaging (UAI) program, which produced an operational prototype in 2004, were Thales Underwater Systems (TUS) and the CSIRO (Commonwealth Scientific and Industrial Research Organisation).

Recent accounts of the overall work have been given by Maguer et al.,<sup>2</sup> Jones,<sup>3</sup> and Vesetas and Manzie.<sup>4</sup> Other aspects of the UAI program have been discussed as follows: rapid signal processing (Blair and Jones<sup>5</sup>; Blair<sup>6</sup>), a simulation of the beamforming process (Blair and Anstee<sup>7</sup>) and near-field beam patterns (Blair<sup>8</sup>).

The system has both a range resolution and a lateral resolution of the order of a few mm per m of range; images can be obtained for ranges from 0.5 m to beyond 2 m. The two-dimensional (2-D) receiving array has a size of a few hundred mm; the array is very sparsely populated and random. A spherical transmitter is used; its center is approximately 50 mm behind the center of the array. The array system has an operating frequency of a few megahertz. For good range resolution the system uses a long chirp pulse combined with ‘dechirping’ through a cross-correlation process (Urlick<sup>9</sup>; Rihaczek<sup>10</sup>). At each receiving element the data stream is digitised using a one-bit quantisation system (Steinberg<sup>11</sup>).

A specular reflector is a surface that reflects waves as a mirror does in optics. Thales Underwater Systems observed in the 1999 ‘Pyrmont 2’ trial that a flat specular reflector can produce what looks like an image of the receiving array (Manzie<sup>12</sup>); we shall call such an ‘image’ a ‘*pseudoimage*.’ That paper also pointed out that the presence of what looks like an image of the array therefore acts as a signature, signalling the presence of a specular reflector.

This paper derives formulae that describe such pseudoimages for both flat and curved reflectors, based on the ‘geometrical approximation.’ In the case of a curved reflector, the formulae assume also the ‘large-range approximation.’ Such formulae have a practical application, namely, that they enable the principal radii of curvature of the reflecting surface to be determined from the acoustic image. A preliminary account of the present work has been given by Blair.<sup>13</sup>

## 2 The observation; geometrical approximation

In the UAI system, when operated in the *fully coherent* mode, beamforming to produce a 3-D image proceeds by combining the signals from all the sensor elements by a standard delay-and-add procedure (Steinberg<sup>11</sup>), using exact path lengths for applicability in the near field (e.g. Knudsen<sup>14</sup>; Blair and Anstee<sup>7</sup>). Strictly speaking, the signals that are combined are the *analytic signals* (Bellanger<sup>15</sup>), represented by a complex number. For each image point  $\mathbf{r}$  (each point in the 3-D image), the absolute value of the resulting complex image amplitude is displayed (coded as brightness or color). The observation of present interest was made in the *partly coherent* mode, in which the array is subdivided into *tiles* and beamforming as above is carried out for each tile. Then, for each image point  $\mathbf{r}$ , the *absolute values* of the image amplitudes due to the various tiles are added together to produce the final image. In this case one discards the information regarding the relative phase of signals from different tiles. As discussed by Vesetas and Manzie,<sup>4</sup> this mode produces an image of lower resolution, but is often used for real-time applications because the image can be computed much more rapidly. Note that for a *fully* coherent array, ‘tile’ is interpreted to mean the whole array. No weighting was applied to the elements.

The present array is made up of square tiles, packed tightly against each other to produce a square lattice; the spacing between tile centers is 50 mm.

In June 1999, the ‘Pyrmont 2’ trial of the then-current UAI system was carried out by Thales Underwater Systems from the DSTO wharf at Pyrmont, Sydney. At one stage a steel plate was imaged; the plate was essentially flat and approximately parallel to the plane of the array. Surprisingly the image, shown in Figure 1, exhibited a pattern of bright ‘spots’ with the regularity of a square lattice (Manzie<sup>12</sup>). That what was observed is, in a sense, an image of the receiving array was confirmed as follows. In the signal processing it was possible to ‘switch off’ one tile at a time. This led to the disappearance of each corresponding spot in turn. It should be noted that the plate had an irregular coating of marine growth (which is actually why the plate was selected). Thus imperfections in the lattice structure, as observed, are to be expected.

In this paper, a partial explanation of the observed results is given, based on the *geometrical approximation*. The latter actually consists of assumptions 1 and 2 as follows. Assumption 1 is that the physical reflection from the surface is described by geometrical acoustics (analogue of geometrical optics). Assumption 2 is that, when the beamforming is subsequently carried out,

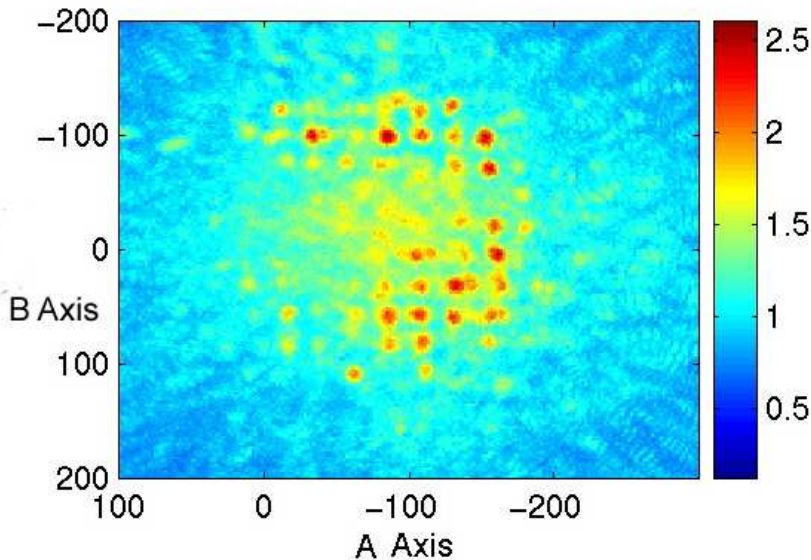


Figure 1: Projection of a 3-D image onto the plane  $\tau$  of the array. The maximum of the image amplitude along a line perpendicular to  $\tau$  is plotted on a linear (not decibel) scale. The origin of the  $ABC$  frame is at the array center. The  $A$  and  $B$  axes are aligned with the tiles. The unit is mm. Reproduced with the permission of Thales Underwater Systems

the  $n$ th element  $R_n$  produces a bright spot in the image at the corresponding *reflecting point*  $S_n$ . Assumption 2 is made plausible by comparing with the case of a point target; then indeed a bright spot appears at the vertex of the go-and-return path. The predicted total pseudoimage is then the collection of the points  $S_n$ .

It is clear that (for a plane reflector parallel to the array plane) the geometrical approximation predicts that the pseudoimage lies on the reflecting surface and is half the size of the array (provided that the transmitter lies in the array plane, as is approximately the case). This is what is observed; in particular, the separations of the spot centers are half the separations of the corresponding tile centers. Robert Vesetas (TUS, private communication) gave the explanation of the observed lattice of spots, implicitly invoking the geometrical approximation.

Assumption 2 places the pseudoimage of  $R_n$  at a definite point. By contrast, exact beamforming would introduce a blurring due to ‘wave’ or diffraction effects. These effects arise because beamforming, with its summing over Huygens wavelets, is an approximation to *backpropagation* (Ljunggren et al.<sup>16</sup>; Shewell and Wolf<sup>17</sup>; Lalor<sup>18</sup>), in which mathematically the wave

reaching the sensors is traced backwards in time.

When a reflecting surface is present, the incoming wave is best thought of as emanating from a point that is the geometrical-acoustics image of the transmitter in the mirror-like surface. Now the beamforming in *range* picks out, as points having a significant image amplitude  $A(\mathbf{r})$ , the points  $\mathbf{r}$  that are on or near the reflecting surface. The overall beamforming therefore should reproduce the wavefront as it was at that surface (immediately after reflection), but cut off in space because the tile has boundaries. Because the backpropagated wave is constricted at the tile, diffraction effects will be produced. When the reflector is in the near field of the tile, we expect Fresnel diffraction to occur: the pseudoimage should be geometrical (having sharp edges) but with slight blurring of the edges (Ditchburn<sup>19</sup>). When the reflector is in the far field,  $A(\mathbf{r})$  should resemble the Fourier transform of the tile, regarded as an aperture (Fraunhofer diffraction, strong blurring). These effects may be described as ‘*numerical diffraction.*’

## 2.1 A subsidiary assumption

Within the strict geometrical approximation, the pseudoimage is predicted to be the same for a partly coherent as for a fully coherent array: the image is predicted to be a seamless square, not the spots of Figure 1! To complete the explanation, we assume that there is some mechanism, caused by the deviation of the true system from strict geometrical behavior, that causes the pseudoimage of a *tile* to be the result of a blurring of the strict geometrical image. Though formally this is an assumption, the above discussion shows that numerical diffraction produces just such an effect. The role of the geometrical approximation, modified by this subsidiary assumption, is to explain the *spacings* in the observed image; the explanation of the image amplitude *profile* of each spot is not attempted in the present paper. (Actually there is a further subsidiary assumption, that the pseudoimage of an *element* is also blurred so that, often or always, the pseudoimages of individual elements cannot be distinguished.)

## 3 Geometry; reflecting surface

### 3.1 Coordinate systems

We define the *chief reflecting point*  $S_0$  of the reflecting surface  $\sigma$  to be such that the normal to  $\sigma$  at  $S_0$  passes through the point transmitter T (Fig. 2). (The theoretical image amplitude function for a *spherical* transmitter is ex-

actly the same as for a point transmitter located at the spherical center.) The normal  $S_0T$ , called the *chief normal*, intersects the plane  $\tau$  of the array at a point  $T_0$ ; the distances  $T_0S_0$  and  $T_0T$  are called respectively the *range*  $r_0$  and the *offset*  $e$ . The *chief tangent plane*  $\mu$  is the tangent plane at  $S_0$ . Let  $\nu$  be the plane, parallel to  $\mu$ , passing through  $T_0$ . A right-handed Cartesian system  $uvw$  is defined with the  $w$  axis along the chief normal and  $v$  along the line of intersection of  $\tau$  and  $\nu$ . (If  $\tau$  and  $\nu$  are the same plane,  $v$  is chosen arbitrarily.) The sense of the  $v$  axis is chosen so that the angle  $\delta$  between  $\tau$  and  $\nu$  lies between 0 and  $\pi/2$  ( $\tau$  must end up lying ‘above’  $\nu$  in Fig. 2).

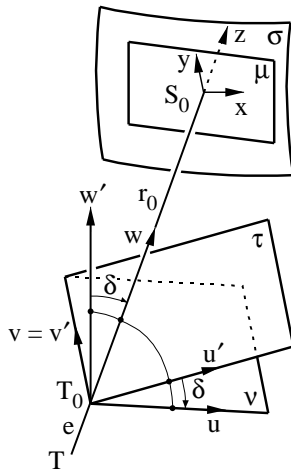


Figure 2: Defining the  $uvw$ ,  $xyz$  and  $u'v'w'$  coordinate systems

A translation of the  $uvw$  axes from  $T_0$  to  $S_0$  yields the  $xyz$  system, with the  $x$  and  $y$  axes lying in the chief tangent plane. By rotating the  $uw$  axes about  $v$  through the angle  $\delta$ , one obtains the  $u'v'w'$  axes, where  $u'$  and  $v'$  lie in the plane of the array. The transformations between the various coordinate systems can be written down from Figure 2. When relating this paper to an experimental image, it will be necessary also to transform from the  $u'v'w'$  frame to a predetermined frame based on the array of sensor elements.

The portion of the reflecting surface  $\sigma$  near  $S_0$  is important because (provided that the transmitter is near the array) only that portion will reflect energy back to the array; energy reaching other parts of  $\sigma$  will not be detected. Let us call  $w'$ , the direction of the array normal, the *broadside* direction. Then the angle  $\delta$  may be thought of as the *departure of  $S_0$  from broadside* when viewed from  $T_0$ . (Note that  $\nu$ , the Greek letter representing the plane, is to be distinguished from  $v$  in  $uvw$ .)

### 3.2 Reflecting surface

The smooth reflecting surface, of the form  $z = f(x, y)$ , is, to first order in  $x$  and  $y$ , simply the tangent plane at  $S_0$ . To the next order,  $z$  is of the form  $z = ax^2 + 2hxy + by^2$ . We assume a surface of exactly this form. By a rotation

$$\begin{bmatrix} X \\ Y \end{bmatrix} = \begin{bmatrix} \cos \alpha & \sin \alpha \\ -\sin \alpha & \cos \alpha \end{bmatrix} \begin{bmatrix} x \\ y \end{bmatrix} \quad (1)$$

to new axes  $X$  and  $Y$ , called the *principal axes*, the equation of the surface may be cast into the form

$$z = \frac{X^2}{2\rho_X} + \frac{Y^2}{2\rho_Y} \quad (2)$$

with no term in  $XY$  (Perlis<sup>20</sup>; Kreyszig<sup>21</sup>; McCrea<sup>22</sup>; Guggenheimer<sup>23</sup>). Here  $\rho_X = 1/\kappa_X$  and  $\rho_Y = 1/\kappa_Y$  are the *principal radii of curvature*. A positive  $\rho_X$  means that the reflecting surface is convex along its intersection with the  $XZ$  plane. For definiteness we choose  $\kappa_X \geq \kappa_Y$  and  $-\pi/2 < \alpha \leq \pi/2$ . The surface is an *elliptic paraboloid* if  $\kappa_X$  and  $\kappa_Y$  are of the same sign and a *hyperbolic paraboloid* if of opposite signs (Spiegel<sup>24</sup>). (In the latter case the origin is a saddle point.) The surface is a *parabolic cylinder* if just one of  $\kappa_X$  and  $\kappa_Y$  is zero and a plane if both are zero. A special case of the elliptic paraboloid, occurring when  $\kappa_X = \kappa_Y$ , is the paraboloid of revolution, to which a *sphere* is a close approximation near  $S_0$ . Similarly an ordinary *cylinder* is a close approximation to the parabolic cylinder.

## 4 Flat reflecting surface

The case of a flat reflector can be solved exactly, subject to the geometrical approximation, to produce a simple result. The geometry is shown in Figure 3; we work in the  $xyz$  coordinate system. Suppose we are given the point  $S(x_s, y_s, 0)$  at which a general ray is reflected (*'reflecting point'*); we obtain the point  $R(x, y, z)$  at which the reflected ray reaches the array plane (*'receiving point'*). First one writes down the coordinates of  $T$  and, using the equality of the angles of incidence and reflection, one obtains  $U$ . From Figure 2 one obtains the equation of the plane  $\tau$ . The point  $R$  where  $SU$  intersects  $\tau$  is then found to be given by

$$\begin{aligned} x &= (2r_0 + e)x_s/D \\ y &= (2r_0 + e)y_s/D \\ z &= -(r_0 + e)(r_0 - x_s \tan \delta)/D \end{aligned} \quad (3)$$



further assumptions, called assumptions 3 and 4. Assumption 3 is that the rays involved in image formation make a small angle with the chief normal (rays are ‘paraxial’). Assumption 4 is that the transmitter and the array may be replaced by their projections, parallel to the chief normal, onto the plane  $\nu$  (Fig. 2).

The calculation is performed in  $XYZ$  coordinates (Fig. 4). Given a point  $S(X_s, Y_s, Z_s)$  on the reflecting surface (2), the incident ray lies along the vector  $\overrightarrow{TS} = (X_s, Y_s, Z_s) - (0, 0, -r_0 - e)$ , where the  $e$  is now dropped because of assumption 4 ( $T = T_0$ ). From (2), a vector normal to the surface at  $S$  is  $(\kappa_X X_s, \kappa_Y Y_s, -1)$ . Let  $\hat{a}$ ,  $\hat{b}$  and  $\hat{c}$  respectively be the unit vectors lying along the incident ray, the normal and the reflected ray, pointing out of the reflector. We now use assumption 3: to first order in  $X_s/r_0$  and  $Y_s/r_0$ , we have

$$\hat{a} = (-X_s/r_0, -Y_s/r_0, -1)$$

$$\hat{b} = (X_s/\rho_X, Y_s/\rho_Y, -1)$$

To first order, the law of reflection is  $\hat{c} = \hat{b} + (\hat{b} - \hat{a})$ , yielding a formula for  $\hat{c}$  in terms of (the position of)  $S$ .

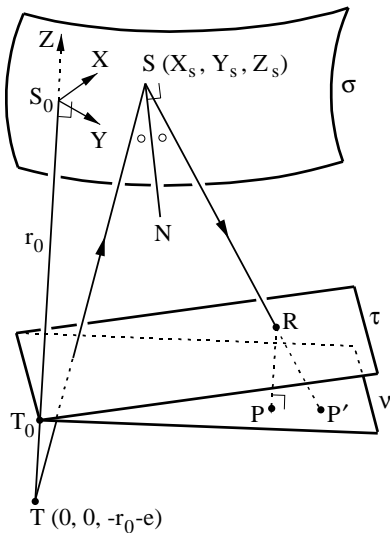


Figure 4: Reflection from a curved surface

We introduce a new coordinate frame  $UVW$ , with axes parallel to the  $XYZ$  axes but with the origin translated from  $S_0$  to  $T_0$  (Fig. 2). From assumption 4, the point of intersection  $P'$  of the reflected ray with the plane

$\nu$  is identified with  $P(U_p, V_p, 0)$ , the projection onto  $\nu$  of the point R on the array that receives the ray from S. By considering the progress of the ray in each of the  $X$  and  $Y$  directions as it traverses the path  $T_0SP'$  it is seen that, to leading order,

$$(U_p, V_p, 0) = r_0(-\hat{a}) + r_0\hat{c} \quad (6)$$

The resulting formulae for  $U_p$  and  $V_p$  in terms of S, when inverted, yield the following formulae for the pseudoimage point in terms of the projected receiver position

$$X_s = m_X U_p, \quad Y_s = m_Y V_p \quad (7)$$

where

$$m_X = \frac{\rho_X}{2(r_0 + \rho_X)}, \quad m_Y = \frac{\rho_Y}{2(r_0 + \rho_Y)} \quad (8)$$

In turn the position  $(U_p, V_p, 0)$  is related to the receiver position  $R(u'_R, v'_R, 0)$  in  $u'v'w'$  coordinates by

$$\begin{bmatrix} U_p \\ V_p \end{bmatrix} = \begin{bmatrix} \cos \alpha & \sin \alpha \\ -\sin \alpha & \cos \alpha \end{bmatrix} \begin{bmatrix} \cos \delta & 0 \\ 0 & 1 \end{bmatrix} \begin{bmatrix} u'_R \\ v'_R \end{bmatrix} \quad (9)$$

From (7) and (8) we see that (the position of) S depends linearly on P; and likewise on R, from (9). Thus the ‘distortion’ in the production of the pseudoimage is a *linear strain*.  $m_X$  and  $m_Y$  will be called the *principal magnifications*. Note that the components of the projected receiver position in the  $X$  and  $Y$  directions are *magnified independently*.

Let  $L$  be the size of the receiving array, equal to the side for a square array and the diameter for an approximately circular array. Let  $f$  be the distance (in 3-D) from the transmitter to the center of the array. Then it can be shown that the conditions (10) to (13) below jointly ensure that assumptions 3 and 4 are good and that the predictions (7), (8) and (9) hold (subject still to the validity of the geometrical approximation):

$$f \lesssim L \quad (10)$$

$$\delta \text{ is not near } \pi/2 \quad (11)$$

$$r_0 \gg L \quad (12)$$

$$|\rho_X + r_0| \gg L \text{ and } |\rho_Y + r_0| \gg L \quad (13)$$

Here (10) means that  $f/L$  is held below some bound of order unity; this allows the transmitter to be outside the array, provided that it is not far outside. Equation (13) entails that radii of curvature too close to  $-r_0$  are not permitted. (Such radii lead to magnifications approaching infinity.) The predictions become increasingly accurate, the better the conditions (12) and (13) are satisfied.

## 5.1 Near-planar reflector

When the reflector is plane one can show, using Equation (5), that the predictions (7), (8) and (9) also hold when the conditions (14) to (17) below are satisfied. Let  $f_1$  be the distance from the center of the array to the projection of the transmitter onto the array plane  $\tau$ . Then the conditions are:

$$f_1 \lesssim L \quad (14)$$

$$|e| \ll r_0 \quad (15)$$

$$\delta \text{ is not near } \pi/2 \quad (16)$$

$$L\delta \ll r_0 \quad (17)$$

Note that we no longer require  $L \ll r_0$  (Eqn 12), only the weaker condition (17). It is believed that the condition that the reflector be plane can be relaxed to the following near-planar condition:

$$|\rho_X| \gg r_0 \text{ and } |\rho_Y| \gg r_0 \quad (18)$$

Indeed, under the conditions (14) to (17), the formulae (5) for the planar reflector reduce to

$$x_s = \frac{1}{2}u' \cos \delta, \quad y_s = \frac{1}{2}v' \quad (19)$$

Thus the magnification from the *projected* array to the pseudoimage is simply  $\frac{1}{2}$ .

## 6 Conditions on the geometrical approximation

Consider first the condition for assumption 1 to hold. In the case of a planar reflector parallel to the array plane, the reflection may be discussed in terms of half-period Fresnel zones (Ditchburn,<sup>19</sup> p. 200; Medwin and Clay<sup>25</sup>). The radius of the central zone, for the reflective case, is  $(r_0\lambda/2)^{1/2}$  where  $\lambda$  is the wavelength (say, the wavelength at the central frequency of the chirp). A similar calculation can be carried out for a nonplanar reflector having magnification  $m_X = m_Y \equiv m$ ; the radius is then  $|mr_0\lambda|^{1/2}$ . Then geometrical acoustics should generally be fairly good in respect of a point  $\mathbf{r}$  in the pseudoimage if  $D_2$  exceeds 2.5 times this radius; here  $D_2$  is the distance from  $\mathbf{r}$  to the nearest edge of the reflector. Now (based on the geometrical approximation) the pseudoimage of a square array is a square, centered on the pseudoimage  $S_1$  of the array center and having side  $|m|L$ . For assumption

1 to be good for the pseudoimage as a whole, let us say it must be good for all points  $\mathbf{r}$  in the circle having center  $S_1$  and radius  $|m|L/2$ . Let  $D_1$  be the distance from  $S_1$  to the nearest edge of the reflector. Then the condition obtained is

$$D_1 \geq \frac{1}{2}|m|L + \frac{5}{2}|mr_0\lambda|^{1/2} \quad (20)$$

For really good accuracy it is reasonable to replace the ‘ $\frac{5}{2}$ ’ by ‘ $\frac{15}{2}$ .’

As a preliminary to discussing assumption 2, we recall from Section 2 that, due to diffraction effects, the pseudoimage of a tile is blurred over some distance  $b$ . Let  $a$  be the side of the (square) tile. The formula for  $b$  depends on whether  $r_0$  is in the near field of the tile ( $r_0 \lesssim a^2/\lambda$ ) (Ditchburn,<sup>19</sup> pp. 211–215) or the far field (together with the transition region) ( $r_0 \gtrsim a^2/\lambda$ ).<sup>11,19</sup> Indeed

$$b \sim \begin{cases} (r_0\lambda)^{1/2} & r_0 \lesssim a^2/\lambda \\ (\lambda/a)r_0 & r_0 \gtrsim a^2/\lambda \end{cases} \quad (21)$$

(These formulae should hold if the magnification  $m$  is of order unity; otherwise  $m$  should enter into the formulae.)

Assumption 2 is good if the pseudoimage is sharp, or ‘geometrical.’ The latter is the case if the blurring distance is small:

$$b \ll L \quad (22)$$

The array size  $L$  is taken as the length for comparison because, as long as (22) holds, the distance between two spots at opposite ends of the array can be determined and hence accurate magnifications obtained (we have again assumed  $m \sim 1$ , so that the pseudoimage size  $mL$  is of order  $L$ ). (Note that, if necessary, an image can be taken with just those two tiles ‘switched on.’)

Note that a different question is whether the pseudoimage of an *individual tile* is sharp, i.e. whether  $b$  is small *on the scale of  $a$* . The condition for this is

$$b \ll a \quad (23)$$

Indeed Figure 1 constitutes an example in which (22) holds but (23) does not.

A similar distinction applies in regard to the conditions (10)–(13) and the conditions (14)–(17). Those conditions apply in respect of the pseudoimage of the array *as a whole*, so that the position of a pseudoimage point is given well if its error is much less than  $mL$ . For the pseudoimage of a single tile to be given well by the relevant approximation, one should replace  $L$  by  $a$  in (10)–(13) and (14)–(17).

Substitution of (21) into (22) yields, as the condition for assumption 2 to hold, a condition of the form ‘(A and B) or (C and D)’. But because  $a \leq L$ ,

it can be shown that the condition reduces to

$$r_0 \ll aL/\lambda \quad (24)$$

If  $a = L/2$  (the largest size of  $a$  allowed by the suggested method), the condition (24) becomes

$$r_0 \ll L^2/\lambda \quad (25)$$

which is more easily satisfied.

Assumption 2 may hold in the following ‘*weak*’ sense when it does not hold in the full sense discussed above. Suppose that the geometrical approximation is being used to estimate, from a pseudoimage, the magnification (and hence the curvature). The weak sense holds if a not-too-bad estimate of the magnification can be made. And in turn, this estimate can be made as long as the above two tile pseudoimages, though blurred, can be resolved as two spots. It follows that the condition for the weak sense to hold has the form

$$r_0 \leq \theta aL/\lambda \quad (26)$$

where  $\theta$  depends on  $m$  but is of order unity when  $m \sim 1$ .

## 7 Comparison with experiment

In the experiment that yielded Figure 1, the range was 1250 mm and the parameter  $r_0/L$  was around 2.5. Both the conditions (20) and (24) for the validity of the geometrical approximation are well satisfied. Because  $r_0/L$  is around 2.5, the large-range condition (12) is not all that well satisfied. However this does not matter, because the reflector is plane and the conditions (14) to (17) *are* well satisfied, the angle  $\delta$  being close to zero. Hence the magnification is predicted to be 0.5, within a few percent. A total error of around 7% is expected when one takes account of the non-clean reflecting surface, which causes spots to be shifted due to refraction. Within this error, the experiment agrees with the ‘0.5’ prediction.

## 8 Conclusions; future work

This paper has derived formulae which, under the appropriate conditions, enable the principal radii of curvature of a specular reflector to be determined from the acoustic image. The fact that such determinations can be made is significant because specular reflectors have traditionally been thought of as ‘hard to image.’

The present work can be extended in two ways. First, one can seek the solution that is exact *within the geometrical approximation*. In outline, the steps are the same as those followed in Section 5 in obtaining the formulae (7) and (8), but with changes as follows. The reflecting surface considered is given exactly by (2). We regard  $x_S$  and  $y_S$  as the independent variables specifying a point  $S(x_S, y_S, z_S)$  on the surface.  $x_S$  and  $y_S$  determine  $X_S, Y_S, Z_S$  and  $z_S$  through Equations (1) and (2).  $\hat{a}, \hat{b}$  and  $\hat{c}$  have the same meanings as before, except that they are expressed in  $xyz$  coordinates;  $\hat{a}', \hat{b}'$  and  $\hat{c}'$  denote the same vectors expressed in  $XYZ$  coordinates. An expression for  $\hat{a}$ , now containing  $e$ , is easily written down. The vector  $\mathbf{b}' = (X_S/\rho_X, Y_S/\rho_Y, -1)$  lies along the normal; its magnitude is  $\hat{b}'$  already defined. Let  $\mathbf{b}$  be related to  $\mathbf{b}'$  by the rotation (1); then  $\hat{b}$  above is  $\hat{b} = \mathbf{b}/|\mathbf{b}|$ .

The law of reflection may be written

$$\hat{c} = 2(\hat{a} \cdot \hat{b})\hat{b} - \hat{a}$$

A general point  $U(x_U, y_U, z_U)$  on the reflected ray, at distance  $t$  from  $S$ , is

$$(x_U, y_U, z_U) = (x_S, y_S, z_S) + \hat{c}t \quad (27)$$

The equation of the array plane  $\tau$  can be written down from Figure 2. Substituting (27) into that equation, we find the value of the parameter  $t$  such that  $U$  coincides with the receiving point  $R$ . Substitution back into (27) gives the  $xyz$  coordinates of  $R$ ; from these the  $u'$  and  $v'$  coordinates can be obtained.

The overall result is a nest of formulae giving the point  $R$  in terms of  $S$ . That result forms a suitable basis for a computer program. By a numerical inversion, such a program would enable  $S$  to be found when  $R$  is given, thus enabling the calculation of pseudoimages.

As noted in Section 2.1, for a full comparison with experiment one needs to go beyond the geometrical approximation by including diffraction effects. Assumption 1—that the physical reflection is described by geometrical acoustics—essentially requires that the smooth reflector be of large extent (Section 6); that assumption should therefore be good under a wide variety of conditions, including those of the present experiment. Consider now the ‘*semigeometrical approximation*,’ which consists in making assumption 1 but not assumption 2; this last point means that the beamforming is treated accurately. The semigeometrical approximation can be applied with or without making a large-range approximation. *With* the latter approximation, one obtains a not-too-complicated formula for the image amplitude as a function of position. *Without* that approximation, one obtains an algorithm from which the image amplitude can be computed. In either case, a comparison can be made with contours such as those in Figure 1, but obtained via a cleaner

experiment. The non-square nature of the ‘spots’ in the present experiment is due to numerical diffraction.

## Acknowledgements

A large part of this work was carried out at the Maritime Operations Division, Defence Science and Technology Organisation, Pirrama Rd, Pyrmont, NSW 2009, Australia. The imaging apparatus was constructed by TUS with the assistance of the Division of Telecommunications, CSIRO. Alexei Kouzoubov of DSTO, Ian S. F. Jones and the referees made useful suggestions for improving the draft.

## References

1. Jones ISF (1996) Underwater acoustic imaging innovation program (DSTO Technical Note DSTO-TN-0065). Aeronautical and Maritime Research Laboratory, Melbourne
2. Maguer A, Vesetas R, Azemard F (2000) 3D acoustic imaging of objects in water. In: Acoustics 2000: Proceedings of Australian Acoustical Society Annual Conference, held at Joondalup Resort, Western Australia, 15–17 Nov. 2000, pp. 87–93. Australian Acoustical Society, Perth, WA
3. Jones ISF (2000) Dimensional images from a high-resolution underwater imager. In: Proceedings of the 32nd Offshore Technology Conference, held at Houston, Texas, 1–4 May 2000, paper 12110. Offshore Technology Conference, Richardson, Texas
4. Vesetas R, Manzie G (2001) AMI: A 3-D imaging sonar for mine identification in turbid waters. In: Oceans, 2001: MTS: IEEE Conference and Exhibition, Honolulu, 5–8 November, 2001, Vol. 1, pp. 12–21. IEEE Press, New York
5. Blair DG, Jones ISF (1998) Underwater acoustic imaging: Rapid signal processing (DSTO Technical Note DSTO-TN-0098). Aeronautical and Maritime Research Laboratory, Melbourne
6. Blair DG (1997) Underwater acoustic imaging: A computing hardware approach to rapid processing (DSTO Technical Note DSTO-TN-0099). Aeronautical and Maritime Research Laboratory, Melbourne
7. Blair DG, Anstee SD (2000) Underwater acoustic imaging: A simulation program and related theory (DSTO Technical Note DSTO-TN-0274). Aeronautical and Maritime Research Laboratory, Melbourne
8. Blair DG (2002) Theory pertaining to comparison and calibration in an experiment to measure acoustic attenuation coefficients (DSTO Technical Note DSTO-TN-0417). Systems Sciences Laboratory, Melbourne
9. Urick RJ (1983) Principles of underwater sound. 3rd ed. McGraw-Hill, New York
10. Rihaczek AW (1985) Principles of high-resolution radar. Revised version. Peninsula, Los Altos, Calif.
11. Steinberg BD (1976) Principles of aperture and array system design—including random and adaptive arrays. Wiley, New York

12. Manzie G (2000) High resolution acoustic mine imaging. In: UDT Pacific 2000: Undersea Defence Technology, Darling Harbour, N.S.W., Australia, 7–9 February, 2000, pp. 356–359. Nexus Information Technology, Swanley, Kent, UK
13. Blair DG (2004) Image due to a curved specular reflector in acoustic mine imaging. In: Proceedings of Mine Countermeasures and Demining Conference, held at Australian Defence Force Academy, Canberra, 9–11 February 2004. Organised by Defence Science and Technology Organisation, Sydney
14. Knudsen DC (1989) A new beamformer for acoustic imaging. In: Oceans '89: An International Conference Addressing Methods for Understanding the Global Ocean. IEEE Press, New York
15. Bellanger M (c. 1984) Digital processing of signals: Theory and practice. Wiley, Chichester, UK, pp. 244–248
16. Ljunggren S, Lovhaugen O, Mehlum E (1980) Sismic holography in a Norwegian fiord. In: Metherell, AE (Ed.), Acoustic imaging: International symposium on acoustical holography and imaging, 1978, Vol. 8, pp. 299–315. Plenum Press, New York
17. Shewell JR, Wolf E (1968) Inverse diffraction and a new reciprocity theorem. *J Opt Soc Am* 58: 1596–1603
18. Lalor E (1968) Inverse wave propagator. *J Math Phys* 9: 2001–2006
19. Ditchburn RW (1952) *Light*. Blackie, London
20. Perlis S (1952) *Theory of matrices*. Addison-Wesley, Cambridge, Mass., pp. 84, 186
21. Kreyszig E (1959) *Differential geometry*. University of Toronto Press, Toronto, pp. 124–134
22. McCrae WH (1960) *Analytical geometry of three dimensions*. Oliver and Boyd, London, pp. 99–101
23. Guggenheimer HW (1963) *Differential geometry*. McGraw-Hill, New York, pp. 209–213
24. Spiegel MR (1968) *Mathematical handbook of formulas and tables*. McGraw-Hill, New York (Schaum's Outline Series), p. 52
25. Medwin H, Clay CS (1997) *Fundamentals of acoustical oceanography*. Academic Press, Boston, Mass., p. 249